THE UNIVERSITY OF MELBOURNE

GMSS – A MATLAB Software Package for Implementing Stochastic Ground Motion Simulations: Version 1.0

By

Yuxiang Tang[1]

16 June 2020

[1] The University of Melbourne, Parkville, Victoria, VIC 3052. Email: tangyuxiang56@gmail.com

Table of Contents

Disclaimer: This program is distributed for academic research sharing purposes only. There is no warranty, expressed or implied, from any individual (including the author Yuxiang Tang) or any institutions or affiliations. Any potential end-users should use this program with caution.

GMSS1.0 is available at: https://github.com/Y-Tang99/GMSS1.0

1. Introduction

The approach of generating accelerograms by the computer through the use of band-limited random signals to represent seismic waves radiated from the source of the earthquake along with modifications of the frequency contents of the radiated waves along their travel path is widely used in engineering seismology as well as in civil and structural engineering. The methodology as described for simulating ground motions is known as stochastic simulations. The frequency content of the simulated accelerograms is controlled by the seismological model. This study is mainly concerned with stochastic simulations of the seismological model for the generation of accelerograms (Boore & Joyner, 1991; Joshi, et al. 1999; Lam, et al. 2000). Many Ground motion models that have been developed for tectonically stable areas are based on this methodology (Boore, 2003).

Stochastic simulation method (or stochastic model) refers to a method of describing the seismic source and path in a partially stochastic, rather than a completely deterministic way (Boore, 2003). The essence of this method described in this study is based on the combination of seismological models (defining the Fourier amplitude of ground motions) with the engineering notion that ground motions are generally random at high frequencies (Hanks & McGuire, 1981). The essential ingredient for stochastic simulation method is the seismological model that contains the physics of the earthquake process and wave propagation.

The translation of a seismological model for simulating accelerograms, or for the development of a GMPE, requires a computer software such as SMSIM (Boore, 2003) or GENQKE (Lam, et al. 2000) for undertaking the simulations. Proper use of such simulation software requires a good understanding of stochastic simulations and the seismological models to avoid misuse of the software. The author favours guiding how to simulate accelerograms on a generic analytical platform using MATLAB, to assist designers and fellow researchers as opposed to offering the program (SMSIM) as a "black box" tool.

The MATLAB package introduced herein is called “GMSS”, which is short for Ground Motion Simulation System or Ground Motion Stochastic Simulation. The package contains three different types of program. The first type (named SSMainPro) is based on wrapper script running in MATLAB and is designed for a single scenario (**M** - **R** combination) simulation. For this type, each step of computation is illustrated in a detailed way, and each parameter value is shown in the workspace in MATLAB to assist the end-users to learn how GMSS is programmed. The second type (MSMainPro) is also based on wrapper script running in MATLAB and is designed for multiple-scenario simulation. The use of this type can facilitate the engineering applications that accelerograms of multiple scenarios are required, e.g. the development of Ground Motion Prediction Equations (GMPEs). The last type (named GMSSPro) is based on the GUI interface and is designed for a user-friendly application. This type can be used as standalone software (but with limitations). Detailed information can be found in the following sections.

2. Seismological Models Used in GMSS

As mentioned above, the seismological model (which is deterministic) is the most important ingredient in the stochastic method. The basic functional form of a seismological model can be expressed as Eq. (1):

$$\mathrm{E}(\mathrm{M}_0, \mathrm{R}, f) = \mathrm{S}(\mathrm{M}_0, f) * \mathrm{G}(\mathrm{R}) * \mathrm{P}(f, \mathrm{R}) * \mathrm{Am}(f) * \mathrm{An}(f) \qquad (1)$$

where $E(M_0, R, f)$ is the target Fourier spectrum; $S(M_0, f)$ is the source factor; $G(R)$ is the geometric spreading (attenuation) factor; $P(f, R)$ is the anelastic whole path attenuation factor; $Am(f)$ is the upper-crust amplification factor; $An(f)$ is the upper-crust attenuation factor; M_0 is defined as the seismic moment in the unit of dyne-cm; f is the frequency of the ground motion in Hz; R is the distance between the source and the site in the unit of km.

2.1 Source factors

Source factors that have been developed to date based on the notion of a "point source" have been reported in the literature (Atkinson & Boore, 1995; Atkinson, 2004; Atkinson & Boore, 2014; Boore, 1983; Brune, 1970). A Point Source Model considers the source of an earthquake as a point from which seismic waves are radiated. If the source of the earthquake is large enough that cannot be regarded as a "point", the point source model may not be capable of representing all the source features of the real earthquake source, and some researchers put forward the finite fault source model. The finite fault model considers the earthquake generating source as a fault that is made up of several sub-faults and each sub-fault can be treated as a point source (Zeng, et al. 1994).

The most commonly accepted source in FAS is represented by the single-corner frequency source factor of (Brune, 1970) which is defined by Eq. (2):

$$S(M_0, f) = (2\pi f)^2 \frac{CM_0}{(1+(f/f_c)^2)} \tag{2}$$

in which, C is the mid-crust scaling factor as defined by Eq. (3) (Atkinson, 1993):

$$C = \frac{R_p F V}{4\pi\rho_0\beta_0^3 R_0} \tag{3}$$

where $R_0 = 1$ km; R_p is the radiation pattern factor (= 0.55), usually averaged over a suitable range of azimuths and take-off angles; F is the free surface amplification factor (= 2.0), and the value of 2.0 strictly speaking is only valid for shear-waves; V represents the partitioning factor of total shear-wave energy into two horizontal components (= $1/\sqrt{2}$); ρ_0 and β_0 are the density and shear-wave velocity (SWV) in the vicinity of the source, and the unit is g/cm^3 and km/s respectively in this study.

Seismic moment M_0 can be expressed in terms of the moment magnitude which is given by Eq. (4) (Hanks & Kanamori, 1979):

$$M = 0.67 \log(M_0) - 10.7 \tag{4}$$

which is the same given by (Boore, et al. 2014) and shown as Eq. (5):

$$\log(M_0) = 1.5M + 16.05 \tag{5}$$

f_c is the corner frequency as defined by Eq. (6) as per the model developed by Brune (1970):

$$f_c = 4.9 \times 10^6 \beta_0 \left(\frac{\Delta\sigma}{M_0}\right)^{1/3} \tag{6}$$

where β_0 is shear wave velocity in km/s, and $\Delta\sigma$ is stress drop in bars.

For large magnitude (M > 6) earthquakes the observed FAS is better modelled by the double corner frequency source factor which was introduced by (Atkinson & Boore, 1995). The basic form of the source factor is defined by Eq. (7):

$$S(M_0, f) = (2\pi f)^2 C M_0 \left[\frac{1-\varepsilon}{1+(f/f_a)^2} + \frac{\varepsilon}{1+(f/f_b)^2}\right] \tag{7}$$

in which parameters in the model are functions of moment magnitude as defined by Eqs. (8a) - (8c) for ENA condition:

$$\log\varepsilon = 2.52 - 0.637\mathrm{M} \tag{8a}$$
$$\log f_a = 2.41 - 0.533\mathrm{M} \tag{8b}$$
$$\log f_b = 1.43 - 0.188\mathrm{M} \tag{8c}$$

The source effects of large earthquakes, including fault geometry, directivity, and slip heterogeneity on the fault plan, can influence the amplitude and duration of ground motions, finite-fault source modelling is important for ground motion prediction, especially for ground motions near the source of large earthquakes (the near-source saturation effects are more obvious for large events at near distances). Motazedian and Atkinson (2005) proposed a finite-fault seismological model based on the concept of the dynamic corner-frequency source model. In this model, the finite-fault source is divided into several sub-faults, and each sub-fault can be regarded as the point source. The finite-fault source model based on dynamic corner frequency can effectively address the near-source saturation effects (distance saturation and magnitude saturation effect). However, the size of sub-fault (or the number of sub-faults) would influence the amplitude estimates of ground motions and thus an additional scaling factor is required (Motazedian & Atkinson, 2005) to remove the sub-fault size impacts. Additionally, Boore (2009a) showed that the point-source model and finite-fault source model can obtain similar simulation results using simple modifications. To avoid the computational cost of the complex finite-fault source model and to achieve similar simulation results for near distance and large magnitudes, Yenier and Atkinson (2014) proposed an "Equivalent Point Source" model. In this model, the source is the point source, and an additional term of pseudo-depth factor (or finite-fault factor) "h_{FF}", which is magnitude dependent, is introduced to consider the ground-motion saturation effects. The functional form of h_{FF} for typical stable continent condition (Boore, et al. 2010) is shown in Eq. (9):

$$h_{FF} = 10^{-0.405+0.235\mathrm{M}} \tag{9}$$

In the generalized double corner frequency source model (Boore, et al. 2014), the f_b value is related to the value of stress drop through the link of single corner frequency f_c , which is corresponding to the observation of recording data, and shown in Eq. (10).

$$f_b = \sqrt{[f_c^2 - (1-\varepsilon)f_a^2]/\varepsilon} \tag{10}$$

An example illustrating the single corner-frequency model and double corner-frequency model is given in Fig. 1.

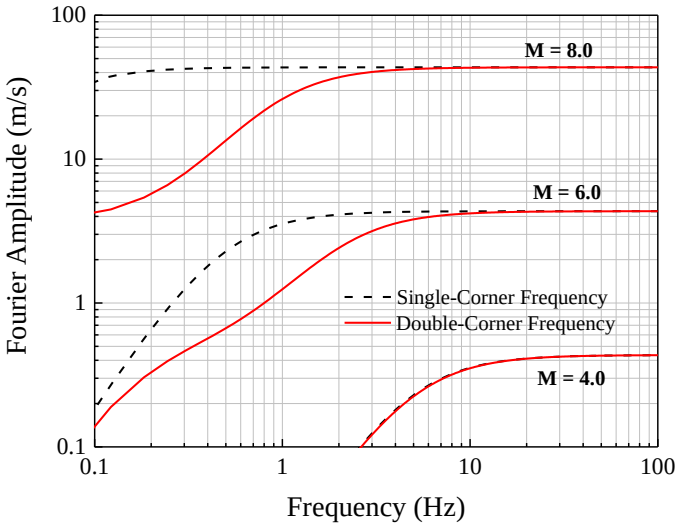

Figure 1. Source spectrum derived from double corner-frequency model and single corner-frequency model ($\Delta\sigma = 200$ bar) for M = 4.0, 6.0 8.0 at R = 30 km.

2.2 Path factors

Path factor, or attenuation factor, is used to describe the spreading characteristics of seismic waves radiated from sources. For most applications, the path effect is represented by simple functions that account for geometric spreading, intrinsic and scattering attenuation (also known as anelastic attenuation), and the general increase of duration with distance due to wave propagation and scattering (considered by path duration) (Boore, 2003). Some examples are given in Table 1 (Boore, 2015) for the path functions (containing geometric spreading and whole path anelastic attenuation factors). Figs. 2 and 3 are the two examples for showing different geometric spreading and anelastic attenuation models, the detailed parameter values for the example attenuation models are shown in Table 1.

Table 1. Example attenuation models for NGA-East

Geometric spreading functions	" R"	" Q "	Applicable range	Model and Reference
$R \le 70, G(R) = R^{-1}$; $70 \le R \le 130, G(R) = 70^{-1} * (\frac{R}{70})^{0}$; $R > 130, G(R) = 70^{-1} * 130^{0} * (\frac{R}{130})^{-0.5}$	$R = R_{hyp}$	$Q(f) = 680f^{0.36}$	$4 \le \mathbf{M} \le 7.25$ $10 \le \mathbf{R} \le 500$ $0.5 \le f \le 20$	**AB95** (Atkinson & Boore, 1995)
$R \le 80, G(R) = R^{-(1.0296-0.0422(M-6.5))}$ $R > 80, G(R) = 80^{-(1.0296-0.0422(M-6.5))} * R^{-0.5*(1.0296-0.0422(M-6.5))}$	$R = R_{hyp}$	$Q(f) = 351f^{0.84}$	$4.5 \le \mathbf{M} \le 8.5$ $1 \le \mathbf{R} \le 400$ $0.1 \le f \le 100$	**SGD02** (Silva, et al.2002)
$R \le 70, G(R) = R^{-1.3}$ $70 \le R \le 140, G(R) = 70^{-1.3} * (\frac{R}{70})^{0.2}$; $R > 140, G(R) = 70^{-1} * 140^{0.2} * (\frac{R}{140})^{-0.5}$	$R = R_{hyp}$	$Q(f) = max\ (1000, 893f^{0.3}$	$4.4 \le \mathbf{M} \le 6.8$ $10 \le \mathbf{R} \le 800$ $0.05 \le f \le 20$	**A04** (Atkinson, 2004)
$G(R) = R^{-1}$, *for all* R	$R = (R_{hyp}{}^2 + h_{FF}{}^2)^{0.5}$, $h_{FF} = 10^{-0.405+0.235M}$	$Q(f) = 2850$	$4.4 \le \mathbf{M} \le 6.8$ $10 \le \mathbf{R} \le 800$ $0.05 \le f \le 20$	**BCA10d** (Boore, et al. 2010)
$R \le 50, G(R) = R^{-1}$; $R > 50, G(R) = 50^{-1} * (\frac{R}{50})^{-0.5}$	$R = R_{hyp}$	$Q(f) = 410f^{0.5}$	$4.4 \le \mathbf{M} \le 5.0$ $23 \le \mathbf{R} \le 602$ $0.2 \le f \le 20$	**BS11** (Boatwright & Seekins, 2011)
$R \le 50, G(R) = 10^{T_C C_{LF}} R^{-1.3}$; $R > 50, G(R) = 50^{-1.3} * (\frac{R}{50})^{-0.5}$ f $\le 1, T_C = 1$; $1 < f < 5, T_C = 1 - 1.429 \log(f)$; $f \ge 5, T_C = 0$. $R \le h, C_{LF} = 0.2 \cos((\pi/2)(R-h)/(1-h))$; $10 < R < 50, C_L = 0.2 \cos((\pi/2)(R-h)/(1-h))$;	$R = (R_{hyp}{}^2 + h_{FF}{}^2)^{0.5}$, $h_{FF} = 10^{-0.405+0.235M}$ h = focal depth	$Q(f) = 525f^{0.45}$	$3.5 \le \mathbf{M} \le 6.0$ $10 \le \mathbf{R} \le 500$ $0.2 \le f \le 20$	**AB14** (Atkinson & Boore, 2014)

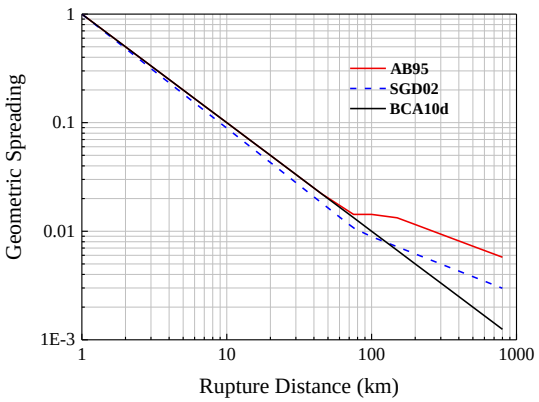

Figure 2. Sample of geometric spreading models

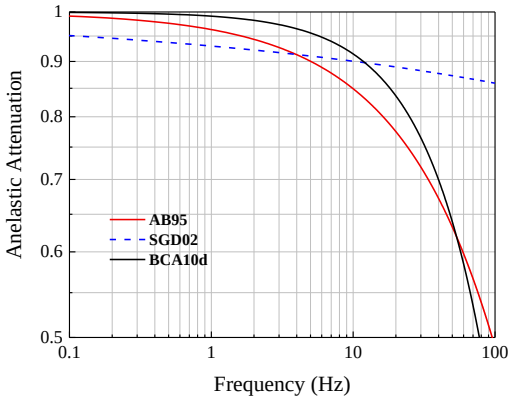

Figure 3. Sample of anelastic attenuation models

It should be noted that if the path functions are determined from recorded/simulated data, it is important to balance the trade-off effects between geometric spreading and anelastic attenuation and the fitting with the data for both. It is important to keep the consistency of geometric spreading and anelastic attenuation functions in practical applications (they need to be adopted from the same seismological model).

Another important part for path factor is the distance-dependent ground motion duration. Because the seismological model itself is not related to duration factor, this will be discussed Section 3.

2.3 Upper-crust modification factors

The study of upper-crust modification effects, on ground motions, is a key topic in engineering seismology.

The upper-crust modification effect is modelled in two separate parts: amplification ($\mathrm{Am}(f)$ in Eq. (1)) and attenuation ($\mathrm{An}(f)$ in Eq.(1)) (same as diminishing) effects. The amplification effect is caused by the difference between the geological conditions of two mediums that shear-wave is propagating. The attenuation effect is used to model the path-independent energy loss of the seismic wave (the path-dependent part is modelled by anelastic attenuation factor).

The amplification factor is expressed as Eq. (13):

$$\mathrm{Am}\,(f) = \sqrt{\frac{\rho_0 \beta_0}{\bar{\rho}_Z \bar{\beta}_Z}} \tag{13}$$

where ρ_0 and β_0 are the density and shear-wave velocity in the vicinity of the source; $\bar{\rho}_Z$ and $\bar{\beta}_Z$ are the time-averaged density and SWV over a depth corresponding to a quarter wavelength. In this study, the units of ρ_0 and β_0 are g/cm^3 and km/s respectively.

$\bar{\rho}_Z$ and $\bar{\beta}_Z$ can be computed from Eqs. (14) and (15) respectively.

$$\bar{\rho}_Z = \left(\int_0^{Z(f)} \rho(Z)\mathrm{d}Z\right)/Z\,(f) \tag{14}$$

$$\bar{\beta}_Z = Z\,(f)/\left(\int_0^{Z(f)} \frac{1}{\beta(Z)}\mathrm{d}Z\right) \tag{15}$$

In Eqs. (14) and (15), $\rho(Z)$ and $\beta(Z)$ is the density and SWV at the depth of "Z" (near the surface). "Z" is defined as the "quarter wave-length" and this method of approximation is called

as “Quarter Wavelength Approximation (QWA)” method (Boore, 2003), which is shown in Eq. (16):

$$\mathrm{Z} = \frac{1}{4}\bar{\beta}/f \tag{16}$$

Combining Eq. (15) and (16), the implicit function of $\mathrm{Z}(f)$ and be expressed as Eq. (17):

$$f(\mathrm{Z}) = 1/[4\int_0^{\mathrm{Z}(f)} \frac{1}{\beta(\mathrm{Z})}\mathrm{dZ}] \tag{17}$$

The upper-crustal amplification factor calculated by Eq. (13) has been proved to be consistent with the wave propagation observations (Boore, 2003; Chen, 2000).

Eq. (13) indicates that SWV profile ($\beta(\mathrm{Z})$) is of significant importance for modelling the site amplification factor.

Two different upper-crust amplification model (mainly for shear-wave velocity profile model) are adopted in GMSS. The first model is based on the reference rock site conditions for generally broad use (which is not proposed for any site-specific conditions) (Boore & Joyner, 1997; Boore, 2016). The second model is proposed for use in site-specific condition and to consider the intra-regional variance of the upper-crust (Tang, 2019).

2.3.1 Reference generic rock site SWV profiling model for use in broad regions

The reference rock site method is widely used in developing modern GMPEs (Atkinson & Boore, 2014; Atkinson, 2004; Atkinson & Boore, 2006; Yenier & Atkinson, 2015; Allen, 2012). Usually, a specific value of V_{S30} (the time-averaged SWV at top 30 m of soil sediment) is determined for a broad target region and the geological settings withing the target region are assumed to be identical. Boore and Joyner (1997) (abbreviated as BJ97 model in the following context) constructed a SWV profiling model as a function of depth for generic rock (GR) site and generic very hard rock (GHR) site, based on borehole data and studies of upper-crustal SWV. Besides, Boore (2016) (abbreviated as B16 model in the following context) put forward a simplified slowness (reciprocal of SWV) interpolation method to construct the SWV profile ($\beta(\mathrm{Z})$)) with specific V_{S30} values using the profiles of GR site (V_{S30} = 0.62 km/s) and GHR site (V_{S30} = 2.78 km/s). The profiling models of GR site and GHR site are summarized in Table 2 and Table 3 respectively.

Table 2. Generic Rock

Depth (km)	**SWV (km/s)**
$\mathrm{Z} \leq 0.001$	0.245
$0.001 < \mathrm{Z} \leq 0.03$	$2.206\mathrm{Z}^{0.272}$
$0.03 < \mathrm{Z} \leq 0.19$	$3.5426\mathrm{Z}^{0.407}$
$0.19 < \mathrm{Z} \leq 4.0$	$2.505\mathrm{Z}^{0.199}$
$4.0 < \mathrm{Z} \leq 8.00$	$2.927\mathrm{Z}^{0.086}$

Table 3. Generic Hard Rock

Depth (km)	**SWV (km/s)**
0.0	2.768
0.05	2.808
0.1	2.847
0.2	2.922
0.5	3.122
0.75	3.260
$0.75 < \mathrm{Z} \leq 2.2$	$3.324\mathrm{Z}^{0.067}$
$2.2 < \mathrm{Z} \leq 8.0$	$3.447\mathrm{Z}^{0.0209}$

The slowness interpolation method proposed by Boore (2016) can be summarized by the following functions from Eqs. (18) to (20).

The relation between slowness and SWV can be shown by Eq. (18):

$$S(Z) = \frac{1}{\beta(Z)} \tag{18}$$

Then a third slowness profile (which is the target profile waiting to be determined) can be derived from the linear interpolation of two generic slowness models (GR and GHR) by Eq. (19):

$$S(Z) = (1-\varepsilon)S_1(Z) + \varepsilon S_2(Z) \tag{19}$$

where $S_1(Z)$ is the slowness of the GR site, and $S_2(Z)$ is the slowness of GHR site at depth of Z km.

The weight coefficient ε can be determined by setting the average slowness equals to the desired value $\bar{S}_D$, and the value of ε can be determined by Eq. (20).

$$\varepsilon = \frac{\bar{S}_D - \bar{S}_1}{\bar{S}_2 - \bar{S}_1} \tag{20}$$

where $\bar{S}_1$ and $\bar{S}_2$ are the average slowness of GR and GHR over top 30 m respectively.

2.3.2 SWV profiling model considering intra-regional variances for site-specific use

Modern Probabilistic Seismic Hazard Analysis (PSHA) needs a higher requirement to deal with the intra-regional variance of upper-crust modification effects. To meet this requirement, Chandler et al. (2005) proposed a generic SWV profiling model which incorporates local geological information to minimize the intra-regional variance. This model is updated by Tang (2019) and validated using field SWV measurements collected from CRUST1.0 database as well as various target subregions (e.g. Melbourne Region and Hong Kong Region). The detailed case-by-case SWV profiling model is summarized in Table 4.

Table 4. Partially non-ergodic SWV profiling model (Tang, 2019)

Case	Depth range (km)	β (km/s)
Case 1 ($Z_S \geq 2$)	$0 < Z \leq 0.2$	$\beta_{0.03}\,(Z/0.03)^{0.3297}$
	$0.2 < Z \leq 2$	$\beta_{0.2}\,(Z/0.2)^{0.1732}$
	$2 < Z \leq Z_S$	$\beta_2\,(Z/2)^{0.1667}$
	$Z_S < Z \leq Z_C$	$\beta_{ZC}\,(Z/Z_C)^n$
	$Z_C < Z$	$\beta_8\,(Z/8)^{0.0833}$
Case 2 ($0.2 < Z_S < 2 \leq Z_C$)	$Z \leq 0.2$	$\beta_{0.03}\,(Z/0.03)^{0.3297}$
	$0.2 < Z \leq Z_S$	$\beta_{0.2}\,(Z/0.2)^{0.1732}$
	$Z_S < Z \leq Z_C$	$\beta_{ZC}\,(Z/Z_C)^n$
	$Z_C < Z$	$\beta_8\,(Z/8)^{0.0833}$
Case 3 ($0.2 < Z_S < Z_C \leq 2$)	$0 < Z \leq 0.2$	$\beta_{0.03}\,(Z/0.03)^{0.3297}$
	$0.2 < Z \leq Z_S$	$\beta_{0.2}\,(Z/0.2)^{0.1732}$
	$Z_S < Z \leq Z_C$	$\beta_{ZC}\,(Z/Z_C)^n$
	$Z_C < Z \leq 2$	$\beta_2\,(Z/2)^{0.0899}$
	$2 < Z$	$\beta_8\,(Z/8)^{0.0833}$
Case 4 ($Z_S < 0.2 < 2 \leq Z_C$)	$0 < Z \leq Z_S$	$\beta_{ZI}\,(Z/Z_I)^{0.3297}$
	$Z_S < Z \leq Z_C$	$\beta_{ZC}\,(Z/Z_C)^n$
	$Z_C < Z$	$\beta_8\,(Z/8)^{0.0833}$
Case 5 ($Z_S < 0.2 < Z_C \leq 2$)	$Z \leq Z_S$	$\beta_{ZI}\,(Z/Z_I)^{0.3297}$
	$Z_S < Z \leq Z_C$	$\beta_{ZC}\,(Z/Z_C)^n$
	$Z_C < Z \leq 2$	$\beta_2\,(Z/2)^{0.0899}$
	$2 < Z$	$\beta_8\,(Z/8)^{0.0833}$
Case 6	$0 < Z \leq Z_S$	$\beta_{ZI}\,(Z/Z_I)^{0.3297}$

($Z_C \leq 0.2$)	$Z_S < Z \leq Z_C$	$\beta_{ZC}\,(Z/Z_C)^n$
	$Z_C < Z \leq 0.2$	$\beta_{0.2}\,(Z/0.2)^{0.2463}$
	$0.2 < Z \leq 2$	$\beta_2\,(Z/2)^{0.0899}$
	$2 < Z$	$\beta_8\,(Z/8)^{0.0833}$

(Z_S and Z_C are the thickness of upper sediment layer and total sediment layers respectively; $\beta_{0.03}$, $\beta_{0.2}$, β_2 and β_8 are the SWV value at the depth of 0.03, 0.2, 2, and 8 km; β_{ZS} and β_{ZC} are the V_S value at the depth of Z_S and Z_C respectively. $Z_I = \min(Z_S, 0.03)$)

In GMSS, the density profile is adopted from the study performed by Brocher (2005). The SWV profiles constructed by BJ model (GR and GHR site) and by Tang (2019) (for Melbourne Region and Hong Kong Region) up to 50 km are shown in Fig. 4 (a), and the corresponding frequency-dependent amplification up to 100 Hz are shown in Fig. 4 (b).

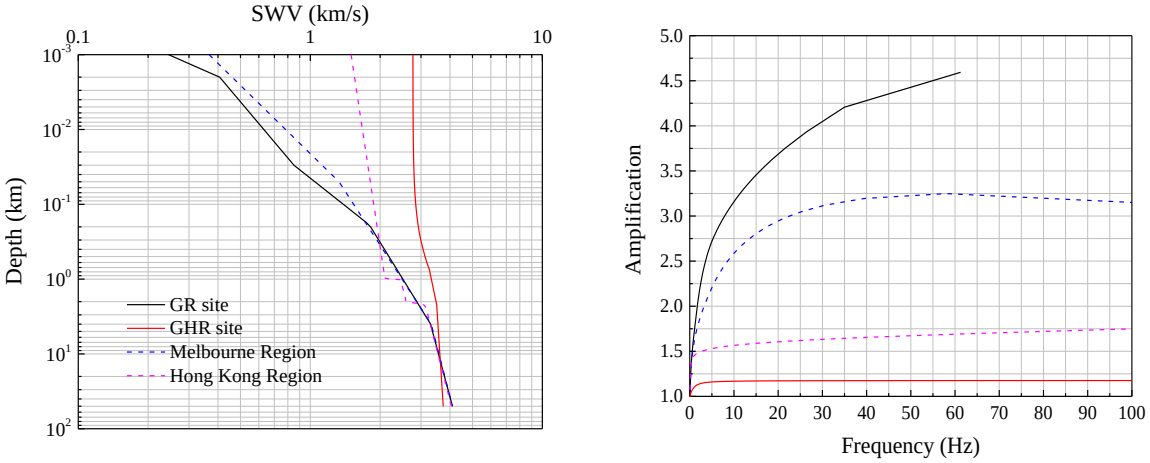

(a) SWV profiles (b) Frequency-dependent amplitude

Figure 4. SWV profiles constructed by BJ model (solid lines) and Tang (2019) model (dash lines), and the corresponding frequency-dependent amplitude factors.

Another important factor of upper-crust modification effect is the upper-crust attenuation factor. The attenuation factor can be represented by two different forms, shown by Eqs. (21) and (22) respectively.

$$\mathrm{An}(f) = [1 + (f/f_{max})^8]^{-1/2} \tag{21}$$

$$\mathrm{An}(f) = \exp(-\pi\kappa_0 f) \tag{22}$$

In this study, both Eqs. (21) and (22) are adopted in the GMSS and users can choose either one based on their preferences.

3. Principles of GMSS

Ground Motion Simulation System or Ground Motion Stochastic Simulation (GMSS) is a MATLAB software package used for generating synthetic accelerograms based on stochastic simulations of seismological models. The particular feature of GMSS is that all the procedures can be run transparently and any user can use it without a solid background of seismology. In this study, three versions of the GMSS software package are provided for different purposes. Version 1 is based on the wrapper script running is mainly designed for random simulation for a single scenario. A very detailed step-by-step explanation of scripts is provided to help the users to understand the whole procedures. Version 2 is also based on wrapper script running and mainly designed for multiple scenarios of ground motion simulations. Users can use this

version to generate synthetic accelerograms for more than one **M**-**R** combination at a time, which is very convenient for developing GMPEs. Version 3 is a standalone software package with a user-friendly interface, and users can get synthetic accelerograms by clicking the mouse, which is convenient for users without any solid seismological backgrounds. All the packages can be downloaded for free and the link can be found in the Data and Resource section. The general procedures of GMSS are illustrated in Fig. 5. Detailed principle of GMSS is introduced step by step in Section 3.1, a user-friendly interface is introduced in Section 3.2.

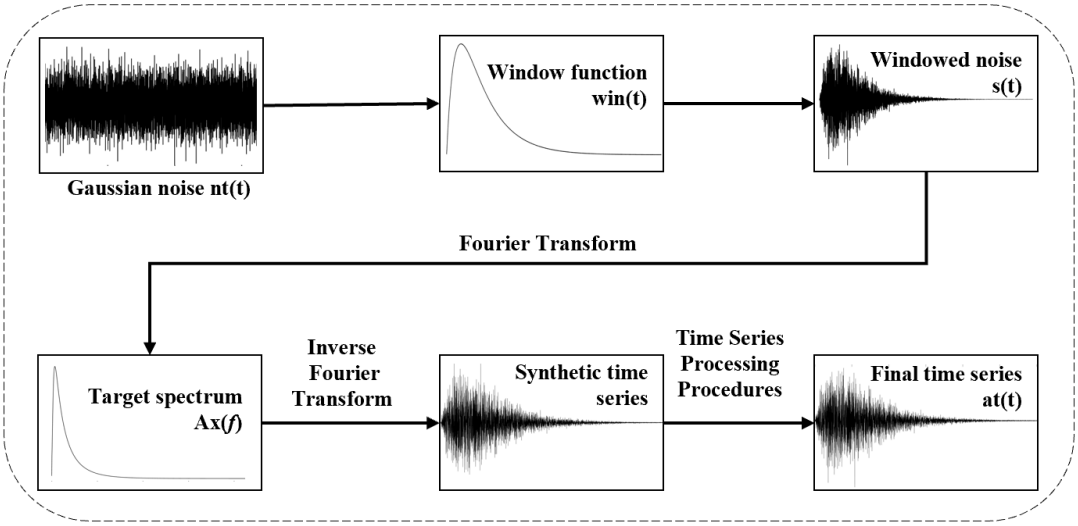

Figure 5. General procedures of synthetic accelerograms generation

3.1 Implementation procedures of GMSS

3.1.1 Generation of Gaussian white noise and filter

Gaussian white noise is used for mimicking the random phenomenon of the seismic waves radiated from the source. Gaussian white noise can be generated by a random number generator that has been built into the computer and can be accessed from many platforms including MATLAB. The white noise must be band-limited in between the lowest frequency value “df” (which is reciprocal of the total duration of the simulated time-history) and the highest frequency (N/2-1) df (Nyquist frequency) where N is the number of time-steps in the simulation.

A 4-level acausal Butterworth filter with a “bandpass” form is adopted in this study. This specific filter is adopted because it is also used in the establishing process of PEER NGA-East Database (Goulet, et al. 2014). Additionally, according to Boore and Akkar (2003), the acausal filter is preferred for the calculation of response spectra, because the results are not dependent on the selected filter frequency.

A typical band-limited Gaussian noise is shown in Fig. 6.

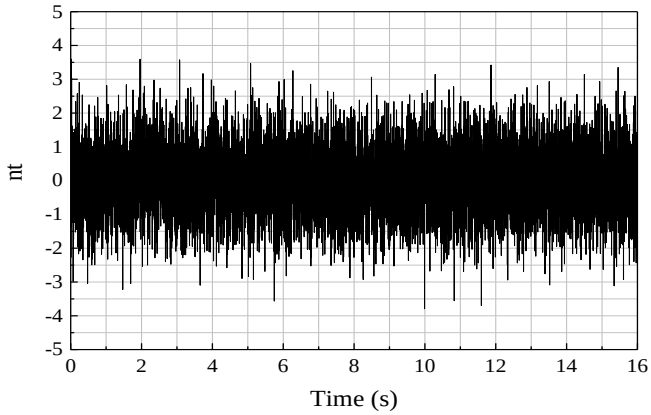

Figure 6 An example of band-limited Gaussian noise

3.1.2 Construction of window function

A window function win(t) is then applied to modulate the signal in the time domain (as shown in Fig. 5).

Essentially,

$$st(t) = win(t) * nt(t) \tag{23}$$

where nt(t) are the band-limited Gaussian noise before the imposition of windowing; win(t) is the imposed time window function which has been scaled in such a way not to alter the overall amplitude of the Gaussian noise. The windowing function win(t) can be of the trapezoidal or exponential form (the window form does not draw many influences on response spectra). The latter has been adopted in this study and is defined by Eq. (24) (Lam et al., 2000):

$$\mathrm{win(t)} = \mathrm{e}^{-0.4\mathrm{t}(6/\mathrm{t_d})} - \mathrm{e}^{-1.2\mathrm{t}(6/\mathrm{t_d})} \tag{24}$$

In the study of Boore (2003), the window function is defined as Eq. (25):

$$\mathrm{win(t)} = 26.312(t/2\mathrm{t_d})^{1.253}\mathrm{e}^{-6.266(\mathrm{t}/2\mathrm{t_d})} \tag{25}$$

Both in Eqs. (24) and (25),

$$\mathrm{t_d} = \mathrm{t_{ds}} + \mathrm{t_{dp}} \tag{26a}$$

$$\mathrm{t_{ds}} = \frac{1}{f_0} \tag{26b}$$

$$\mathrm{t_{dp}} = \mathrm{b}\mathbf{R} \tag{26c}$$

where $\mathrm{t_d}$ is the total ground motion duration, and $\mathrm{t_{ds}}$ is source duration, $\mathrm{t_{dp}}$ is path duration (as mentioned in Section 2.2). f_0 is corner frequency (can be single-corner or double-corner), **R** is the distance, and b is a distance-dependent coefficient. If the source model is single-corner frequency model, f_0 equals to f_c (defined as Eq. (6)). If the source model is double-corner frequency model, f_0 would be changed into the two corner frequencies defined by Eqs. (8) and (12) with suitable weights of the two corner-frequencies. The distance-dependent duration (path duration) is an important factor as well because the peak ground motions will decrease with distance increases. Empirical observations and theoretical simulations suggest that path duration can be modelled by several connected straight-line segments (Boore, 2003). In this study, b would be fixed at 0.05 at all distances for simplicity if no further information is given. The final function of $\mathrm{t_d}$ can be represented as Eq. (27).

$$t_d = 0.5\frac{1}{f_a} + 0.5\frac{1}{f_b} + 0.05\mathbf{R} \quad (27)$$

In GMSS, users can define the path duration for real situations by inputting the self-defined input file.

The window functions win(t) described by Eqs. (24) and (25) are shown in Fig. 7, in which t_d is assumed to be 10 s for both functions.

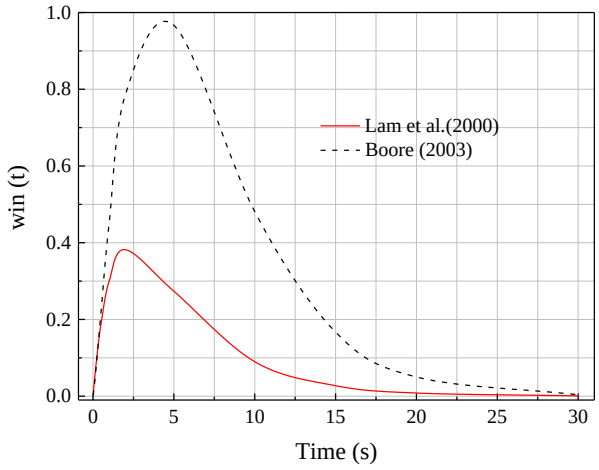

Figure. 7 Window function win(t), t_d = 10 s for both functions

st(t) in Eq. (22) is the windowed noise and there is an ensemble of such noise time series with random variability within them. An example of st(t) is illustrated in Fig. 8.

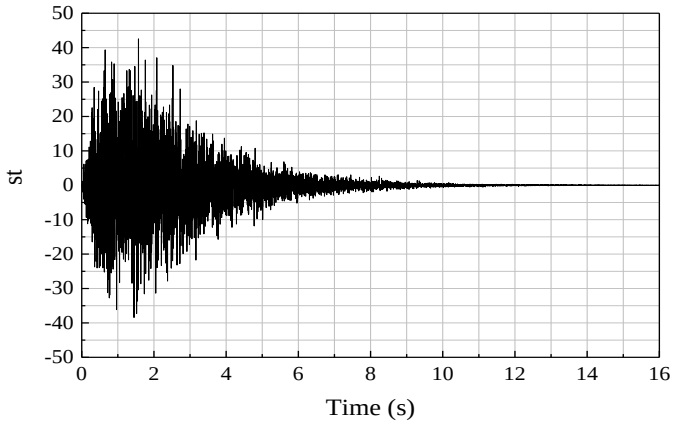

Figure 8. An example of windowed noise st(t)

3.1.3 Fourier Transform of windowed noise

In this study, the built-in "Fast Fourier Transform (fft)" function in MATLAB is adopted to perform the Fourier transform of the windowed white noise. The purpose of the Fourier transform is to find the Fourier amplitudes of the windowed noises, which have random variability within different simulations and are averaged to unity across the simulated accelerogram ensembles. The set of phase angles obtained from the Fourier transform is reserved for use in the inverse Fourier transform procedure to remove any possible

uncertainties introduced in the two procedures (fast Fourier transform and inverse Fourier transform). The basic expressions of "fft" function in MATLAB and the inverse process can be expressed as Eqs. (28a) and (28b).

$$\mathrm{X(k)} = \sum_{r=1}^{N} x(r)\exp\left(-j2\pi(k-1)(r-1)/N\right) \quad (28a)$$

$$\mathrm{x(r)} = (1/\mathrm{N})\sum_{k=1}^{N} X(k)\exp\left(j2\pi(k-1)(r-1)/N\right) \quad (28b)$$

where X(k) is the Fourier amplitude signal and x(r) is the original signal, N is the total number of the time step.

After the Fourier transform, the spectrum of the noise is noted as As(*f*). An example spectrum is shown in Fig. 9.

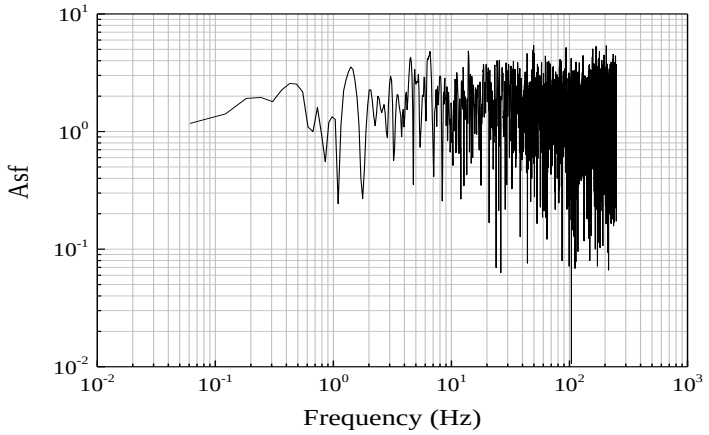

Figure 9. An example of a noise signal after Fourier Transform As(*f*)

3.1.4 Target spectrum and filtered spectrum

The seismological model identified in Section 2 is the frequency filter Ax(*f*) which defines the frequency content of the ground motion in the form of a Target Fourier Amplitude Spectrum as illustrated in Fig. 5. A summary of the well-publicized, and established, seismological models (including source models, attenuation functions, and upper-crust modification factors) has been presented in Section 2. More detailed introduction to the concept of seismological modelling can be found in the study performed by Boore (2003).

Next step is filtering windowed noise signal (As(*f*)) by the seismological model Ax(*f*) - Fourier Amplitude Spectrum. Aa(*f*) is essentially a product of As(*f*) and Ax(*f*). Aa(*f*) obtained from an individual simulation may contain considerable random variabilities. Importantly, the ensemble-averaged Aa(*f*) as derived from repetitive simulations should display convergence to Ax(*f*). An example of Target spectrum ($\Delta\sigma$ = 200 bar**,** **M** = 6, **R** = 30 km, Q_0 = 680, *n* = 0.36, no upper-crust modification effect), Ax(*f*), and the filtered spectrum Aa(*f*) are shown in Fig. 10.

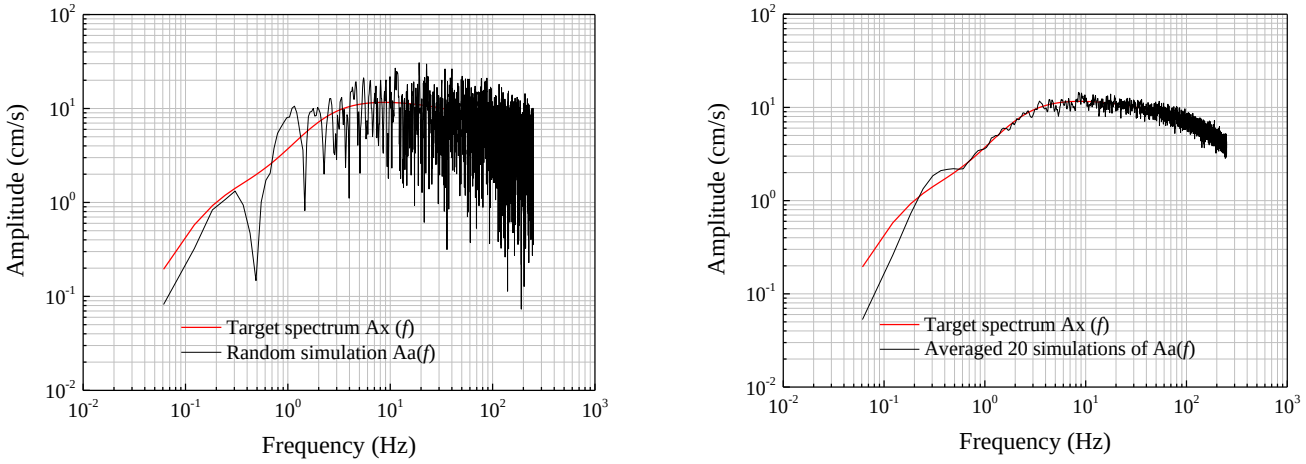

(a) One random simulation

(b) average of 10 random simulations

Figure 10. An example of the target spectrum and random simulations

It is important to perform the procedures stated above in the order strictly, otherwise, some unexpected results would be obtained. For example, if the noise nt(t) is filtered by a seismological model Ax(*f*) first and then windowed by window function win(t), the long-period level of the motion will be distorted, and this result is also reported in Boore (2003).

3.1.5 Generation of time series and time series processing procedures

The next step is the inverse Fourier Transform of the windowed-filtered noise signal – Inverse Fourier Transform of Aa(*f*) whilst incorporating the phase angles obtained from Fourier Transform to give the ground motion time-series a(t). This procedure is straightforward and simple. However, the time series obtained from the procedures stated above cannot be used for engineering applications directly. Further time series processing procedures are required to obtain a more reliable time series.

According to Boore (2005), response spectra and peak ground motions should be computed from the complete, padded time series, not from the pad-stripped data directly. Pad-stripped time series which are provided by data agencies can be misleading for computing peak ground motions or response spectra. The ground-motion intensity measures such as peak velocity and response spectral amplitudes provided by the agencies which are obtained from the complete padded and filtered acceleration time series may be different from the computed results based on the pad-stripped time series. This also implies that using the pad-stripped time series for any analysis, such as the response of a nonlinear structure, is inconsistent use of the time series (Boore, 2009b). The time series of recorded data in the NGA database are always pad-stripped data. One reason for only providing pad-stripped time series might be because plots of the padded and filtered accelerations would appear to have a long section of zero motion before the arrival of the shaking, and users might be tempted to remove this section of the time series. Doing so, however, may lead to distortions in quantities such as peak displacements and oscillator response derived from the truncated time series (Boore, et al. 2012). The time series of accelerograms generated by an original program like GENQKE and SMSIM (the version before 2002) is just like the pad-stripped data in the database.

Baseline correction, or zeroth-order correction, is also required which should be combined with the filter, to help to obtain the correct simulations. In this study, a sixth polynomial fit to the trend is computed as the baseline correction that is removed from the original time series of

acceleration. Moreover, 20-second pre-event and after-event time pads are added to the time series to ensure the displacement time series will not distort at long durations.

For calculating the time series of velocity and displacement, the general approach is numerical integration. The Northbridge integration method is adopted for the purpose. Refer Fig. 11 for a typical sample of the simulated time series which are presented in the form of the acceleration, velocity and displacement formats, for before and after TSPP.

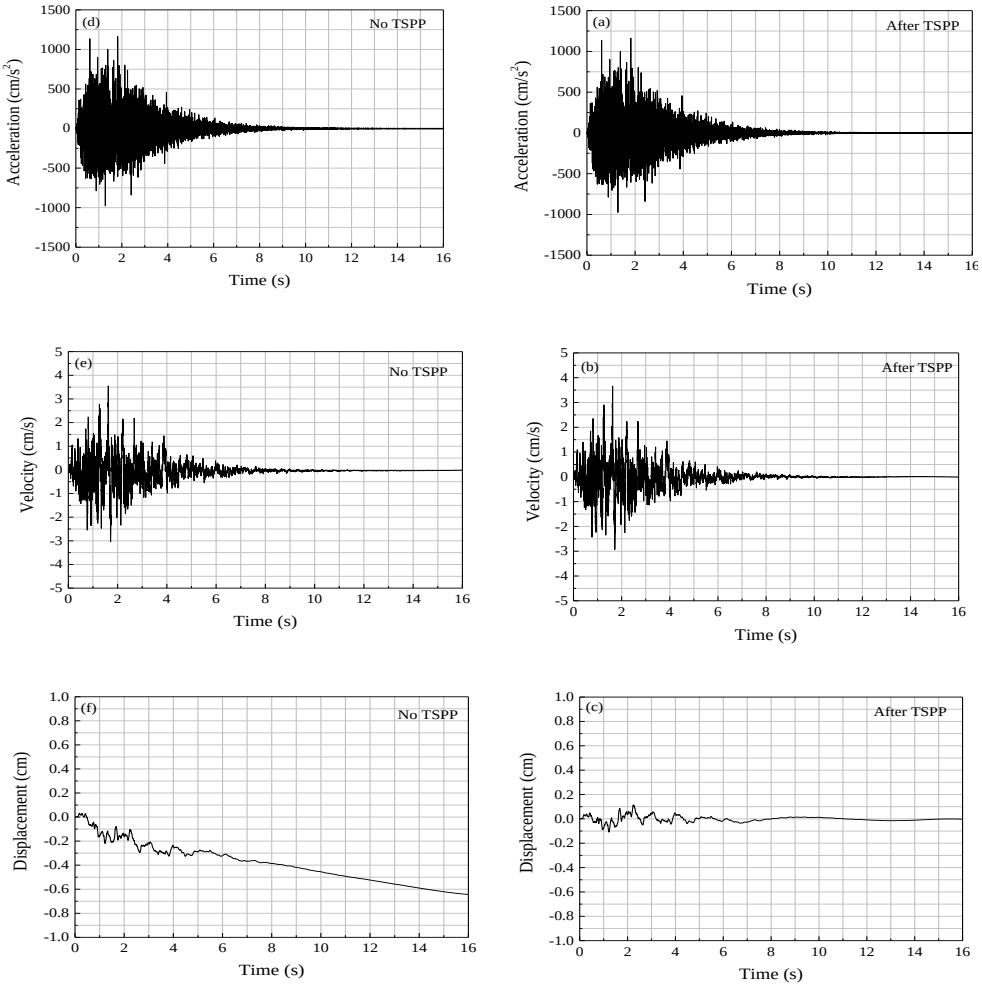

Figure 11. Simulated ground motion time series, before and after Time Series Processing Procedures (TSPP), the time-pad is not shown.

3.1.6 Computation of response spectra

By definition, the response spectrum (it can be acceleration, velocity or displacement) describes the maximum response of a single-degree-of-freedom (SDOF) oscillator to a specific input ground motion. Response spectrum does not describe real ground motion, and it only provides information on how SDOF oscillators respond to the input ground motion. Structures are usually approximated by SDOF oscillators in engineering practice and structures with different heights correspond to the oscillators with different natural circular frequency (F_n) or natural periods (T_n). Response spectrum is a function of the natural circular frequency and damping ratio (ξ) of a suite of SDOF oscillators. In practice, the damping ratio (ξ) is assumed to be the same for all oscillators (Robinson, et al. 2006).

Analytical solution of the equation of motion for a SDOF system is usually not possible if the excitation (applied force or ground acceleration) varies arbitrarily with time or if the system is nonlinear. Such problems can be tackled by numerical time-stepping methods for integration of differential equations (Chopra, 2 007). The time-stepping method, namely the Central Difference Method (CFD), will be adopted to construct the response spectrum in this study. Detailed mathematic expressions can be found from Eqs. (29) to (33).

Getting started from the dynamic equation of a simple SDOF system:

$$m\ddot{u} + c\dot{u} + ku = p(t) \tag{29}$$

If time step integration method is adopted, Eq. (28) can be expressed as Eq. (30):

$$m\ddot{u}_i + c\dot{u}_i + ku_i = p(t_i) \tag{30}$$

Eq. (30) can be obtained by dividing the mass from both sides of Eq. (31):

$$\ddot{u}_i + 2\xi\omega_n\dot{u}_i + \omega_n^2 u_i = -\ddot{u}_{gi} \tag{31}$$

Eq. (31) can be obtained from the definition of "slope":

$$\dot{u}_i = \frac{u_{i+1} - u_{i-1}}{2\Delta t} \tag{32a}$$

Similarly,

$$\ddot{u}_i = \frac{u_{i+1} - 2u_i + u_{i-1}}{\Delta t^2} \tag{32b}$$

Finally, Eq. (33) can be obtained by combining Eqs. (31) and (32):

$$u_{i+1} = \frac{-\ddot{u}_{gi} + \left(\frac{2}{\Delta t^2} - \omega_n^2\right)u_i + \left(\frac{\xi\omega_n}{\Delta t} - \frac{1}{\Delta t^2}\right)u_{i-1}}{\frac{1}{\Delta t^2} + \frac{\xi\omega_n}{\Delta t}} \tag{33}$$

This is the foundation of the calculation of displacement response spectrum, and using the relationship between displacement and velocity, acceleration, all response spectra can be computed. The detailed meaning of each parameter shown in Eqs. (29 - 33) is given in Table 5.

Table 5. Parameters used in the Central Difference Method

Parameter	Meaning	Unit
m	Structure mass	kg
c	Viscous damping	/
k	Structure stiffness	/
$\ddot{u}$	Ground motion acceleration	m/s^2
$\dot{u}$	Ground motion velocity	m/s
u	Ground motion displacement	m
$p(t)$	External excitation	N
ξ	Damping ratio (as a proportion of critical damping value)	/
ω_n	Angular velocity	rad/s
Δt	Time interval	s

3.1.7 Construction of Conditional Mean Spectrum (CMS)

Scenario-specific median response spectra would need to be predicted using GMSS to account for regional conditions of the upper-crust. CMS (Baker, 2011) is then constructed using Eq. (34):

$$\mu_{\ln RSA(T_i)} = \mu_{\ln RSA}(M, R, T_i) + \rho(T_i, T^*)\varepsilon(T^*)\sigma_{\ln RSA}(T_i) \quad (34)$$

where $T^*$is reference natural period ; $\mu_{\ln RSA(T_i)}$ is target response spectral value at period T_i (in natural logarithmic unit); $\mu_{\ln RSA}(M, R, T_i)$ is median prediction of the same by GMSS at the period T_i; $\sigma_{\ln RSA}(T_i)$ is standard deviation at the period T_i; $\varepsilon(T^*)$ is the difference between the target response spectral value (RSA^*) and the median prediction by GMSS at T^* as defined by Eq. (35); $\rho(T_i, T^*)$ is the correlation coefficient for the value of $\varepsilon(T)$ as defined by Eq. (36) (Baker & Jayaram, 2008).

$$\varepsilon(T^*) = \frac{\ln RSA^* - \mu_{\ln RSA}(M,R,T^*)}{\sigma_{\ln RSA}(T^*)} \quad (35)$$

$$\rho(T_i, T^*) = 1 - \cos\left[\frac{\pi}{2} - 0.359 \ln \frac{\max(T_i, T^*)}{\min(T_i, T^*)}\right] \quad (36)$$

Case studies can be found in companion papers (Tang, 2019; Tang, et al. 2020).

3.2 User-friendly interface platform

To make the whole simulation process more user-friendly, a user-interface platform is developed. The platform is developed using the MATLAB GUI and can be used as standalone software. The detailed information on how to use the MATLAB guide to design GUI platform can be found on the website of Mathworks (http://www.mathworks.com/products/compiler). The overall programming flowchart is shown in Fig. 12, the programming flowchart of the site-specific SWV profiling model (Tang 2019) is shown in Fig.13, and the final user-interface is shown in Fig. 14.

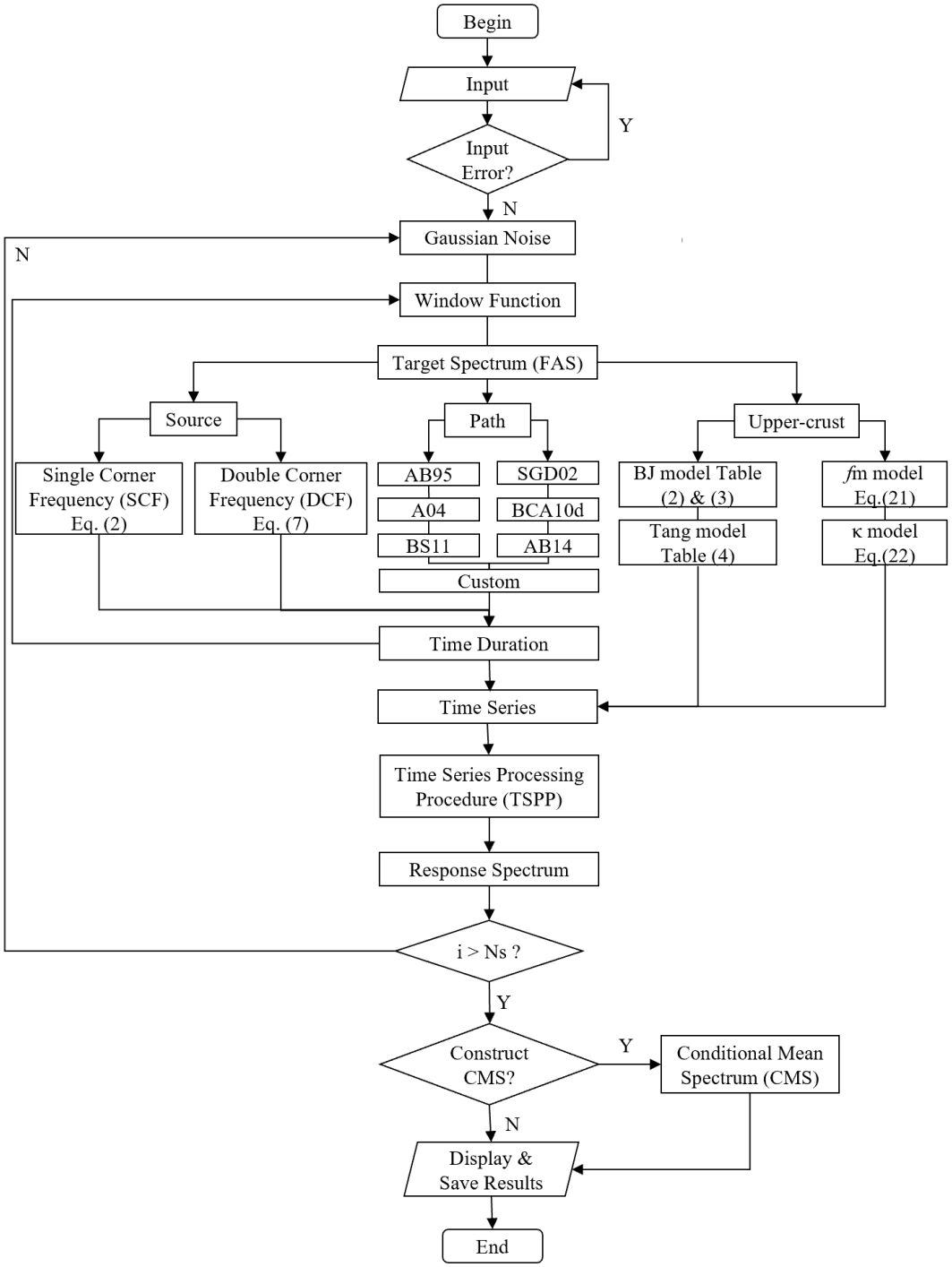

Figure 12. Overall programming flowchart of GMSS

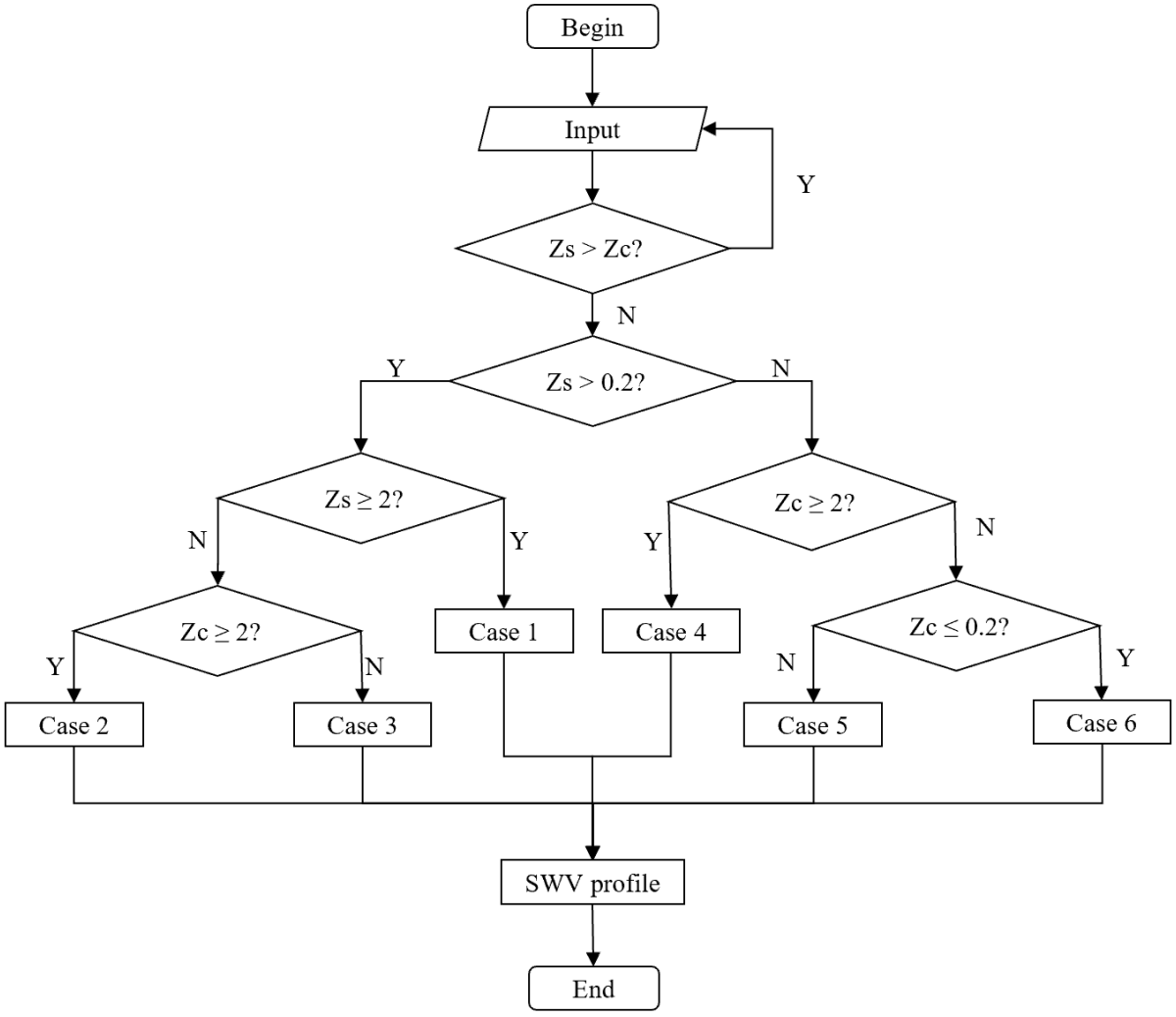

Figure 13. Programming flowchart of site-specific SWV profiling model (Tang, 2019). The detailed SWV profiling model for each Case can be found in Table 4.

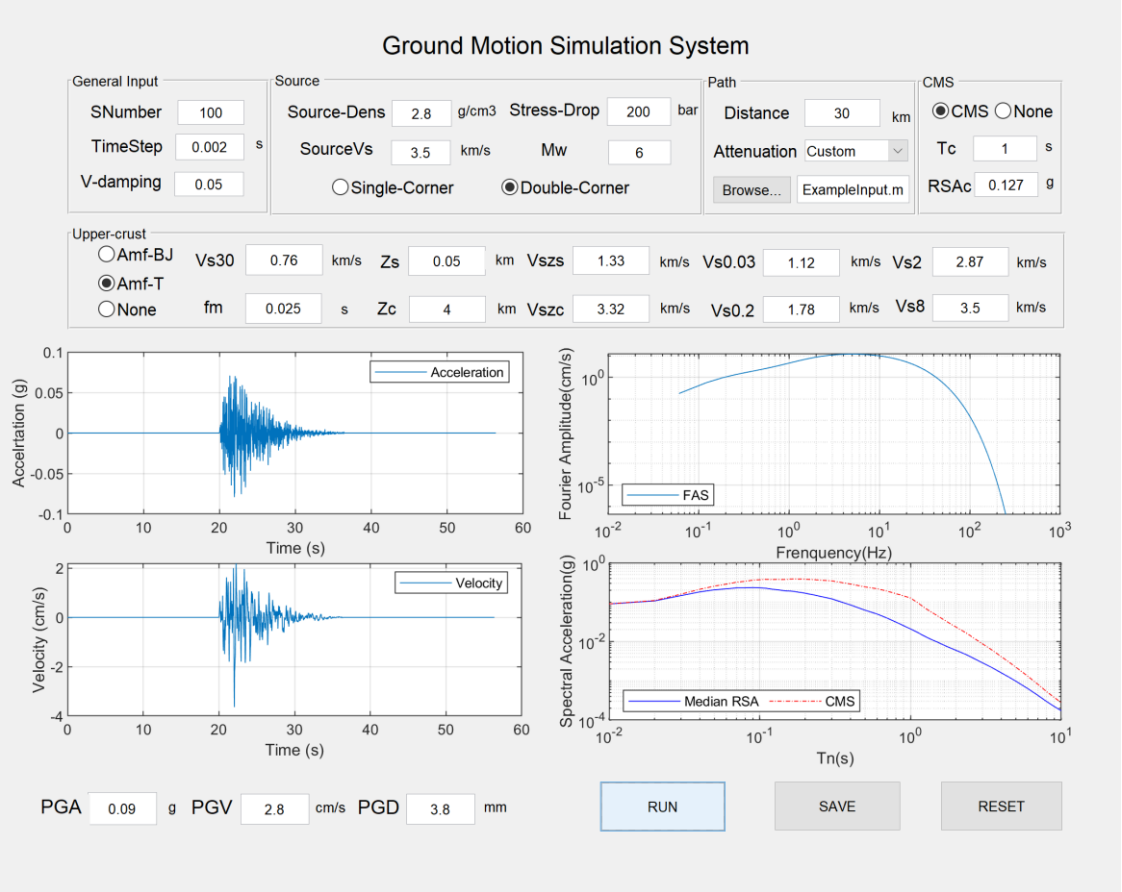

Figure 13. User-interface of GMSS

The detailed explanation of each symbol shown in Fig.14 is given in Table 6.

Table 6. Definition of symbols used in GMSS

Symbol	Definition
SNumber	Number of simulations, which is 100 by default
TimeStep	Time interval/step used in GMSS, which is 0.002 s by default, and no larger than 0.02 is recommended
V-damping	Viscous damping value, which is 0.05 by default
Source-Dens	Source density, which is 2.8 g/cm^3 by default
SourceVs	Source shear-wave velocity, which is 3.5 km/s by default
Stress-Drop	Brune stress drop, which is 200 bar by default
Mw	Moment magnitude, which is 6 by default
Single-Corner	Single-corner-frequency source model, which is shown in Eq. (2)
Double-Corner	Double-corner-frequency source model, which is shown in Eq. (7)
Distance	Hypocentral distance if no more information is given, which is 30 km by default
Attenuation	Ground motion attenuation functions, including geometric spreading function and while-path anelastic attenuation function. Default functions are adopted from Table 1. Users can input self-defined function by clicking the “Browse…” button and select an input file
CMS	This radio button is for constructing Conditional Mean Spectrum for ground motion and selection purposes. Eqs. () to () are used in GMSS
None	This radio button means no CMS is required and the result returns the median value of RSA
Tc	Conditioning natural period

RSAc	Conditioning RSA, usually obtained from Code spectrum or Uniform Hazard Spectrum
Amf-BJ	Site amplification function which is proposed by Boore and Joyner (1997) and Boore (2016) for reference rock site (Section 2.3.1)
Amf-T	Site amplification function which is proposed by Tang (2019) for site-specific use (Section 2.3.2)
None	No site amplification is used
Vs30	Time-averaged shear-wave velocity at top 30 m, which is 0.76 km/s by default (as a referenced rock site for WNA and SEA)
fm	Site attenuation factor, which is 0.025 s by default proposed by Yenier and Atkinson (2014). If fm > 1, Eq. (20) would be used in GMSS, and if fm < 1, fm would equal to κ and Eq. (21) would be used
Zs	The thickness of the upper sedimentary crust layer, which is 0.05 km by default (for Melbourne condition)
Zc	The thickness of total sedimentary crust layer, which is 4 km by default (for Melbourne condition)
Vszs	The shear-wave velocity at the depth of Zs km, which is 1.33 km/s by default (for Melbourne condition)
Vszc	The shear-wave velocity at the depth of Zc km, which is 3.32 km/s by default (for Melbourne condition)
Vs003	The shear-wave velocity at the depth of 0.03 km, which is 1.12 km/s by default (for Melbourne condition)
Vs02	The shear-wave velocity at the depth of 0.2 km, which is 1.78 km/s by default (for Melbourne condition)
Vs2	The shear-wave velocity at the depth of 2 km, which is 2.87 km/s by default (for Melbourne condition)
Vs8	The shear-wave velocity at the depth of 8 km, which is 3.5 km/s by default (for Melbourne condition)
PGA	Peak ground acceleration, in the unit of "g"
PGV	Peak ground velocity, in the unit of "cm/s"
PGD	Peak ground displacement, in the unit of "mm"

The outputs of GMSS include time series of ground motions, PGA, PGV, PGD, Fourier amplitude spectrum and response spectra. All the calculation results can be saved into an EXCEL spreadsheet directly by clicking the "SAVE" button. The input parameters, peak ground motions, Fourier Amplitude Spectrum, time series (maximum save 100 simulations per time), and response spectra as well as CMS (if needed) will be saved. Fig. 14 shows an example input file and Fig.15 shows an example output file.

```
%This file is used for defining the attenuation functions by users.
%The output of this file woould be the distance-dependent paraemeters,
%including geomeritc spreading factor, whole-path anelastic attenuation
%factor, and path duration factor.
%-------------------------------------------------------------------------
% DO NOT CHANGE ANY PARAMETER SYMBOLS

%^^^^^^^^^^^^^^^^^^^^^^^^^^^^^^^^^^^^^^^^^^^^^^^^^^^^^^^^^^^^^^^^^^^^^^^^
%^^^^^^^^^^^^^^^^^^^^^^^^^^^^^^^^^^^^^^^^^^^^^^^^^^^^^^^^^^^^^^^^^^^^^^^^
f=getappdata(0,'f');                                    %^^
beta=str2double(get(handles.SourceVs, 'String'));       %^^
R=str2double(get(handles.Distance, 'String'));          %^^
M=str2double(get(handles.Mw, 'String'));                %^^
%^^^^^^^^^^^^^^^^^^^^^^^^^^^^^^^^^^^^^^^^^^^^^^^^^^^^^^^^^^^^^^^^^^^^^^^^
%^^^^^^^^^^^^^^^^^^^^^^^^^^^^^^^^^^^^^^^^^^^^^^^^^^^^^^^^^^^^^^^^^^^^^^^^
% Example functions for Switzerland
% Whole-path anelastic attenuation factor

Q=270*f.^0.5; Q=Q.*beta; Q=Q.^(-1);

% Geometric spreading factor

%If there is a finite-fault factor, hFF=10^(-0.405+0.235*M);
% R=sqrt(hFF^2+R^2);
if R<=70
    G=R^(-1.11);
elseif R<=120
    G=(70^(0.41)/(70^1.11))*R^(-0.41);
else
    G=(70^(0.41)/70^(1.11))*(120^(1.38)/120^(0.41))*R^(-1.38);
end

% Path duration
if R<=100
    tdp=0.153*R;
else
    tdp=0.02*(R-100)+15.3;
end
```

Figure 14. Example input file.

Simulation No.	100
Time Step(s)	0.002
Source Density(g/cm^3)	2.8
Source SWV(km/s)	3.5
Stress Drop(bar)	200
Magnitude	6
Distance(km)	30
Vs30(km/s)	0.76
fm(s)	0.025
Damping Value	0.05
Zs(km)	0.05
Zc(km)	4
Vszs(km/s)	1.33
Vszc(km/s)	3.32
Vs003(km/s)	1.12
Vs02(km/s)	1.78
Vs2(km/s)	2.87
Vs8(km/s)	3.5
Tc(s)	1
RSAc(g)	0.127

Sheet1 | FAS | At | Vt | Dt | RSA | MedianRSA&CMS

Figure 15. Example output file. The input parameter values are saved in “Sheet1”; Peak ground motions (PGA, PGV, and PGD) and Fourier amplitude spectrum are saved in “FAS”; Time series of acceleration, velocity and displacement are saved in “At”, “Vt” and “Dt” respectively (maximum 100 simulations can be saved per run); Response spectral acceleration is saved in “RSA” (maximum 100 simulations can be saved per run); Median value of response spectral acceleration and Conditional mean spectrum (if have) are saved in “MedianRSA&CMS”

The standalone GMSS version (GMSSPro) needs to be installed in the PC before running. In the installation package, “for testing” can be run before installation if “MATLAB Runtime (for MATLAB version R2019b)” has been installed in the computer.

Acknowledgements

The continuous guidance and support from Prof. Nelson Lam at The University of Melbourne are sincerely acknowledged. The support from A. Prof. Hing-Ho Tsang at Swinburne University of Technology is deeply acknowledged. The assistance provided by Dr Elisa Lumantarna at The University of Melbourne in related research work is also acknowledged

References

Allen, T. I. (2012). Stochastic ground-motion prediction equations for southeastern Australian earthquakes using updated source and attenuation parameters. Canberra.

Atkinson, G., & Boore, D. (1995). Ground-Motion Relations for Eastern North America. Bulletin of the Seismological Society of America, 85, 17-30.

Atkinson, G. M. (2004). Empirical Attenuation of Ground Motion Spectral Amplitudes in Southeastern Canada and the Northeastern United States. Bull. Seismol. Soc. Am., 94, 1079-1095.

Atkinson, G. M., & Boore, D. M. (2006). Earthquake Ground-Motion Prediction Equations for Eastern North America. Bull. Seismol. Soc. Am., 96(6), 2181-2205.

Atkinson, G. M., & Boore, D. M. (2014). The attenuation of Fourier amplitudes for rock sites in eastern North America. Bull. Seism. Soc. Am, 104, 513-528.

Atkinson, G. M., & Boore, D. M. (2014). The Attenuation of Fourier Amplitudes for Rock Sites in Eastern North America. Bull. Seismol. Soc. Am., 104(1), 513-528.

Boatwright, J., & Seekins, L. (2011). Regional Spectral Analysis of Three Moderate Earthquakes in Northeastern North America. Bull. Seism. Soc. Am, 101, 1769-1782.

Baker, J.W. 2011. Conditional Mean Spectrum: Tool for Ground-Motion Selection, Journal of Structural Engineering, Vol 137(3) 322-331.

Baker, J.W. and Jayaram, N., (2008) "Correlation of spectral acceleration values from NGA ground motion models," Earthquake Spectra, 24(1), 299-317.

Boore, D. (1983). Stochastic simulation of high-frequency ground motions based on seismological models of the radiated spectra. Bull. Seism. Soc. Am, 73, 1865-1894.

Boore, D. M. (2003). Simulation of Ground Motion Using the Stochastic Method. Pure Appl. Geophys., 160, 635-676.

Boore, D. M. (2005). On Pads and Filters: Processing Strong-Motion Data. Bull. Seism. Soc. Am., 95(2), 745-750.

Boore, D. M. (2009a). Comparing Stochastic Point-Source and Finite-Source Ground-Motion Simulations: SMSIM and EXSIM. Bull. Seismol. Soc. Am., 99(6), 3202-3216.

Boore, D. (2009b) TSPP---A Collection of FORTRAN Programs for Processing and Manipulating Time Series. U.S. Geological Survey Open-File Report 2008-1111: USGS.

Boore, D. M. (2015). Point-Source Stochastic-Method Simulations of Ground Motions for the PEER NGA-East Project.

Boore, D. M. (2016). Short Note: Determining Generic Velocity and Density Models for Crustal Amplification Calculations, with an Update of the Boore and Joyner (1997) Generic Amplification for Vs(Z)=760 m/s. Bull. Seismol. Soc. Am., 106(1), 316-320.

Boore, D. M., & Akkar, S. (2003). Effect of causal and acausal filters on elastic and inelastic response spectra. Earthquake Engng Struct. Dyn., 32, 1729-1748.

Boore, D., Sisi, A. A., & Akkar, S. (2012). Using Pad-Stripped Acausally Filtered Strong-Motion Data. Bulletin of the Seismological Society of America, 102, 751-760.

Boore, D. M., Alessandro, C. D., & Abrahamson, N. A. (2014). A Generalization of the Double-Corner-Frequency Source Spectral Model and Its Use in the SCEC BBP Validation Exercise. Bull. Seismol. Soc. Am., 104(5), 2387-2398.

Boore, D. M., Campbell, K. W., & Atkinson, G. M. (2010). Determination of stress parameter for eight well-recorded earthquakes in eastern North America. Bull. Seismol. Soc. Am., 100, 1632-1645.

Boore, D. M., & Joyner, W. B. (1991). Estimation of Ground Motion at Deep-Soil in Eastern North America. Bull. Seism. Soc. Am., 81(6), 2167-2185.

Boore, D. M., & Joyner, W. B. (1997). Site Amplifications for Generic Rock Sites. Bull. Seismol. Soc. Am., 87(2), 327-341.

Brocher, T. M. (2005). Empirical Relations between Elastic Wavespeeds and Density in the Earth's Crust. Bull. Seismol. Soc. Am., 95(6), 2081-2092.

Brune, J. N. (1970). Tectonic stress and the spectra of seismic shear waves from earthquakes. J. Geophys.Res, 75, 4997-5009.

Chandler, A. M., Lam, N. T. K., & Tsang, H. H. (2005). Shear wave velocity modelling in crustal rock for seismic hazard analysis. Soil Dynamics and Earthquake Engineering, 25, 167-185.
Chen, S. (2000). Global Comparisons of Earthquake Source Spectra. (Doctor of Philosophy), Carleton University, Ottawa, Ontario, Canada.
Chopra, A. K. (2007). Dynamics of structures Theory and applications to earthquake engineering (Third ed., pp. 171-173). New Jersy: Pearson Education Inc.
Goulet, C. A., Kishida, T., Ancheta, T. D., Cramer, C. H., Darragh, R. B., & Silva, W. J. (2014). PEER NGA-East Database. Retrieved from Pacific Earthquake Engineering Research Center.
Hanks, T. C., & Kanamori, H. (1979). A moment magnitude scale. J. Geophys.Res, 84(B5), 2348-2350.
Hanks, T. C., & McGuire, R. K. (1981). The Character of High-frequency Strong Ground Motion. Bull. Seism. Soc. Am., 71, 2071-2095.
Joshi, A., Kumar, B., Sinvhal, A., & Sinvhal, H. (1999). Generation of synthetic accelerograms by modelling of rupture plane. Journal of Earthquake Technology, 36(1), 43-60.
Lam, N. T. K., Wilson, J., & Hutchinson, G. (2000). Generation of Synthetic Earthquake Accelerograms Using Seismological Modelling: A Review. Journal of Earthquake Engineering, 4(3), 321-354.
Motazedian, D., & Atkinson, G. M. (2005). Stochastic Finite-Fault Modeling Based on a Dynamic Corner Frequency. Bull. Seismol. Soc. Am., 95(3), 995-1010.
Robinson, D., Dhu, T., & Schneider, J. F. (2006). SUA: A computer program to compute regolith site-response and estimate uncertainty for probabilistic seismic hazard analyses. Computers & Geosciences, 32, 109-123.
Silva, W., Gregor, N., & Darragh, R. (2002). Development of Regional Hard Rock Attenuation Relations for Central and Eastern North America. Report to Pacific Engineering and Analysis.
Tang, Y. (2019). Seismic Hazard Analysis and Management for Low-to-moderate Seismicity Regions Based on Ground Motion Simulation. (Doctor of Philosophy), The University of Melbourne, Melbourne, Victoria, Australia.
Tang, Y., Lam, N. T. K., Tsang, H. H., & Lumantarna, E. (2019). Use of Macro-seismic Intensity Data to Validate a Regionally Adjustable Ground Motion Prediction Model. Geosciences, 9(10), 1-22. doi:http://doi.org/10.3390/geosciences9100422
Tang, Y., Lam, N. T. K., Tsang, H. H., & Lumantarna, E. (2020). An Adaptive Ground Motion Prediction Equation for Use in Low-to-moderate Seismicity Regions. Journal of Earthquake Engineering, Accepted.
Tang, Y., Lam, N. T. K., Tsang, H. H. (2020). A Computational Tool for Scaling Strong Motion Accelerograms Incorporating Regional Crustal Conditions. Seismo. Res. Letts., Submitted.
Yenier, E., & Atkinson, G. M. (2014). Equivalent Point-Source Modeling of Moderate-to-Large Magnitude Earthquakes and Associated Ground-Motion Saturation Effects. Bull. Seismol. Soc. Am., 104(3), 1458-1478.
Yenier, E., & Atkinson, G. M. (2015). Regionally Adjustable Generic Ground-Motion Prediction Equation Based on Equivalent Point-Source Simulations: Application to Central and Eastern North America. Bull. Seismol. Soc. Am., 105(4), 1989-2009.
Zeng, Y., Anderson, J., & Yu, G. (1994). A composite source model for computing realistic synthetic strong ground motions. Geophys. Res. Lett., 21, 725-728.